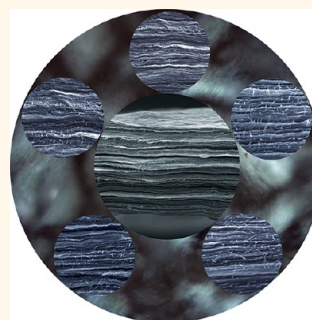# Organic Solvent-Based Graphene Oxide Liquid Crystals: A Facile Route toward the Next Generation of Self-Assembled Layer-by-Layer Multifunctional 3D Architectures

Rouhollah Jalili,[†,§] Seyed Hamed Aboutalebi,[‡,§] Dorna Esrafilzadeh,[†] Konstantin Konstantinov,[‡] Simon E. Moulton,[†] Joselito M. Razal,[†] and Gordon G. Wallace[†,*]

[†]Intelligent Polymer Research Institute, ARC Centre of Excellence for Electromaterials Science and [‡]Institute for Superconducting and Electronic Materials, AIIM Facility, Innovation Campus, University of Wollongong, North Wollongong, NSW 2522 Australia. [§]These authors contributed equally to this work.

ABSTRACT We introduce soft self-assembly of ultralarge liquid crystalline (LC) graphene oxide (GO) sheets in a wide range of organic solvents overcoming the practical limitations imposed on LC GO processing in water. This expands the number of known solvents which can support amphiphilic self-assembly to ethanol, acetone, tetrahydrofuran, N-dimethylformamide, N-cyclohexyl-2-pyrrolidone, and a number of other organic solvents, many of which were not known to afford solvophobic self-assembly prior to this report. The LC behavior of the as-prepared GO sheets in organic solvents has enabled us to disperse and organize substantial amounts of aggregate-free single-walled carbon nanotubes (SWNTs, up to 10 wt %) without compromise in LC properties. The as-prepared LC GO-SWNT dispersions were employed to achieve self-assembled layer-by-layer multifunctional 3D hybrid architectures comprising SWNTs and GO with unrivalled superior mechanical properties (Young's modulus in excess of 50 GPa and tensile strength of more than 500 MPa).

Lyotropic liquid crystalline (LC) phases in dispersions containing two-dimensional graphene and graphene oxide (GO) sheets have added a new dimension to soft self-assembly science.[1−9] Soft self-assembly of materials, which is the route for engineering of amphiphilic molecules into different supermolecular assemblies in one, two, or three dimensions, has been of interest for decades.[10−12] Fields such as nanomedicine, biocatalysis, bioactive delivery systems, self-assembled composites, and solar cells have taken advantage of the self-organization of amphiphilic molecules in recent years.[13−16] Recently, a series of graphene-based macroscopic structures including paper and fibers have been fabricated employing the novel amphiphilic soft self-assembly route.[1,4,17] The much expected enhancement in properties, self-assembly, and alignment of GO might be achieved if the simultaneous dispersion of functional materials with GO in the liquid crystalline media is realized.[18] To date, the application of graphene-based liquid crystals as a promising building block in different fields has not yet been realized mainly because of the practical limitations induced by water, the only medium in which the formation of LC GO has been reported. However, there are limitations for aqueous media to disperse many nanomaterials that would be expected to introduce enhanced properties to LC GO. For example, the introduction of highly debundled, isolated, and self-oriented carbon nanotubes (CNTs), which has only been observed in CHP and never in water with LC GO, would be expected to enhance electrochemical and mechanical properties. Understanding and manipulating the forces involved in amphiphilic self-assembly and expanding the range of solvents in which such phenomena can be exploited will enable the development of new composites based on LC GO.[10]

Here we report the ability to support GO lyotropic LC phase formation in a wide range of organic solvents through the use of ultralarge GO sheets. This approach enables the exploitation of the LC order of GO sheets in organic solvents to organize and align single-walled carbon nanotubes (SWNTs). This work has enabled self-assembly of ultrastiff, ultrastrong three-dimensional (3D) GO-SWNT architectures with high elongation-at-break.

RESULTS AND DISCUSSION

Formation of LC GO in Various Organic Solvents. To date, water is recognized as the practical medium for the self-assembly of GO.[19] In the pursuit of rationally designed lyotropic LC GO dispersions in various organic solvents, we dispersed ultralarge GO sheets in a number of common solvents including water, *N,N*-dimethylformamide (DMF), *N*-cyclohexyl-2-pyrrolidone (CHP), tetrahydrofuran (THF), acetone, ethanol, and a number of other organic solvents, many of which were not known to afford solvophobic self-assembly prior to this report. The organic solvents, successfully used here, can support dissolution or dispersion of a wide range of materials. This means that self-assembly of a variety of compositions in the solvent media that support LC GO formation would be possible. For example, DMF and THF are the most common solvents for processing polymers. Therefore, dispersing GO in these solvents and achieving LC GO would provide unique opportunities in the production of self-assembled, fully ordered, and novel LC GO-based polymer composites. LC GO in THF might also be used as an ordered template for the synthesis and self-assembly of metallic nanoparticles such as boron or magnesium, which are water- and air-sensitive. LC GO in CHP, being the best known solvent for debundling CNTs,[20] might promote fabrication of fully ordered self-assembled CNT-GO composites containing highly debundled CNTs. Ethanol and acetone are general purpose solvents, which are commonly used as building blocks in organic chemistry. Acetone is also the solvent of choice for a wide range of epoxy families. Therefore, attaining LC GO in acetone would open an avenue for novel self-assembled epoxy-based nanocomposites. Other solvents in which we observed lyotropic LC formation of GO include ethylene glycol, methanol, acetonitrile, isopropyl alcohol, *N*-methyl pyrrolidone (NMP) and dimethyl acetamide (DMAc). All of the nonpolar solvents were ineffective in dispersing GO and therefore could not afford any LC phase as expected. Representative polarized optical microscopy (POM) micrographs of the representative solvents are given in Figure 1. POM micrographs clearly show the birefringent lyotropic LC behavior of GO in water and all of the above-mentioned organic solvents (see also Supporting Information Figures S1–S6). The transition concentration from isotropic to the nematic phase was experimentally found to be ~0.25 mg mL^{-1} for water,
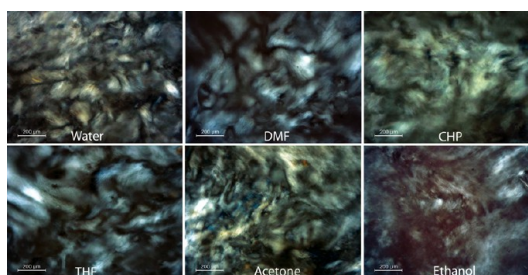
Figure 1. Representative cross-polarized optical microscopy of LC GO in various organic solvents at a GO concentration of 2.5 mg mL^{-1}.

TABLE 1. LC Formation Concentration and GO Sheet Properties in Different Solvents

solvent	LC formation concentration (mg mL^{-1})	sheet thickness[a] (nm)	*d*-spacing[b] (nm)
water	0.25	0.83	0.825
DMF	0.25	1.1	1.05
CHP	0.25	1.0	0.101
THF	0.50	0.92	0.937
acetone	0.50	0.86	0.846
ethanol	0.25	0.83	0.820

[a] Obtained from AFM images. [b] Obtained from XRD patterns.

DMF, CHP, and ethanol and ~0.50 mg mL^{-1} for acetone and THF (Table 1). At higher concentrations, the nematic phase formed in all of the solvents spontaneously. Depending on the concentration, as-prepared organic LC GO can be either stable for months or undergo what is stated as degradation.[21] It should be noted that these concentrations, although the lowest filler content ever reported for the formation of liquid crystals from any colloid, are still higher than the theoretical biphasic region between 0.05 to 0.09 mg mL^{-1} calculated for rigid platelets (see Supporting Information for details). This discrepancy can be attributed to the flexible nature of the monolayer GO sheets and their tendency of wrinkling especially in the presence of attached functional groups.

Characterization of LC GO. Atomic force microscopy was employed to assess the number of layers and quality of GO sheets in the organic solvent-based LC dispersions (Figure 2). No aggregation or restacking of GO sheets was observed in any solvent investigated here. As-prepared GO dispersions in all of the organic solvents contained GO sheets that are predominantly in the size of more than tens of micrometers. Step height measurements performed on the samples indicated that all of the samples contained single-layer GO sheets, as the mean measured height was between 0.8 and 1.2 nm depending on the solvent used. The thickness of a monolayer of graphene is about 0.34 nm;[22] however, GO has functional groups that act as pillars giving rise to the larger measured height. Some solvent molecules are also expected to bond with the surface of GO and remain even after drying.
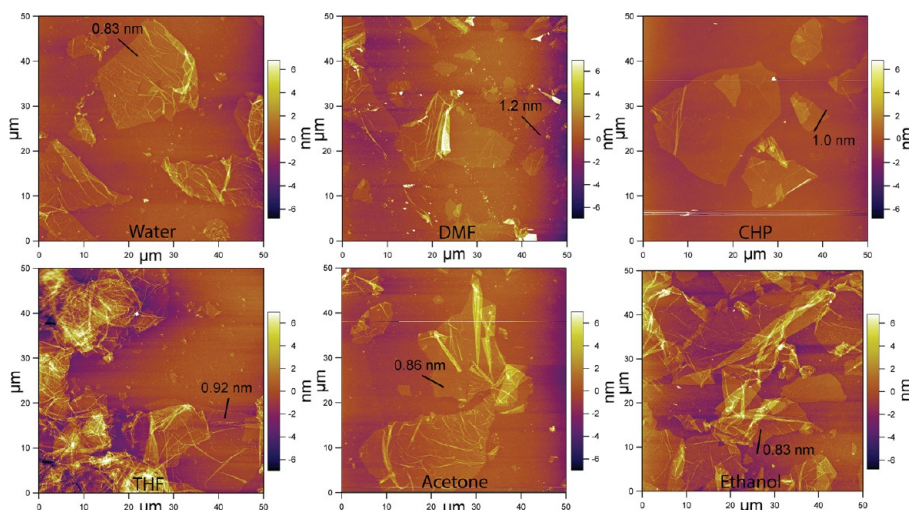
Figure 2. AFM images of GO sheets prepared from various organic solvent-based LC GO dispersions. Marked line in each image shows the measured thickness of the sheet.

Hydrogen bonding of each solvent molecule with GO resulted in different apparent sheet thickness, depending on the solvent molecular size and arrangement on the surface of GO sheets. Moreover, the crumpling of GO sheets that occurs in the case of THF (Figure 2) might also result in lower effective aspect ratio which manifests itself in the observation of different phase boundaries presented in Table 1.

The change in the apparent thickness of GO sheets as a result of bonding with different solvents can also be confirmed by measuring the interlayer d-spacing of GO sheets in cast dried films made from various solvent-based GO (Table 1). The d-spacing represents the interlayer distance between individual GO sheets in the paper material that are oriented perpendicularly to the diffraction plane. XRD measurements were performed to evaluate the effect of the solvents on the interlayer d-spacing of GO films (Figure 3a). The process of making GO in water or organic solvents is accompanied by an increase in the d-spacing between the graphene layers from about 0.34 nm to ≈0.8−1.1 nm, which is related to the degree of oxidation and the hydration level (in the case of GO prepared in water) or the bonding of other solvent molecules to graphene sheets.[1,23−26] Therefore, the peak in the XRD patterns of our as-prepared GO films corresponds to the layer-by-layer distance (d-spacing) of each sample prepared in each organic solvent according to the Bragg's law. The position of the peak and correspondingly the d-spacing values observed in the XRD patterns varied with the solvent used. The differences on d-spacing values could be attributed to the confinement of organic solvent molecules in the lamellar GO sheet layers, as in the case of water for aqueous LC GO dispersions. This result could be illustrated by the larger d-spacings for GO sheets when dispersed in acetone, THF, CHP, and DMF, which had intersheet distances of 0.978, 1.01, and 1.17 nm, respectively, than
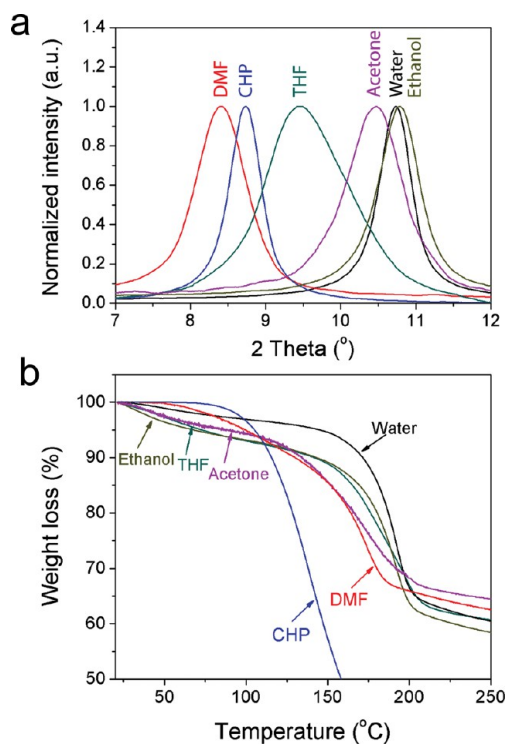
Figure 3. (a) X-ray diffraction patterns (XRD) and (b) thermal gravimetric analysis (TGA) of GO films as a function of solvents.

that of GO in water (0.846 nm). A very small shift (d-spacing 0.820 nm) was observed in ethanol-based LC GO, consistent with the similarity of size with water. The measured d-spacing values were also in good agreement with the measured GO sheet thickness from AFM results (Table 1). Therefore, we suggest that the individual GO platelets are interlinked *via* a nonuniform network of hydrogen bonds mediated by oxygenated functional groups and solvent molecules.

Thermal gravimetric analysis (TGA) was also performed on GO papers (Figure 3b). GO papers which

were cast from organic solvents with high boiling point temperatures (154 and 153 °C for CHP and DMF, respectively) lost considerably more weight at higher temperatures compared to GO recovered from water. In contrast, GO dispersed in volatile solvents (acetone, THF, and ethanol) started to lose weight at much lower temperatures. This behavior can be attributed to the confinement of solvent molecules between GO sheets during film formation. The variation between the final weight losses was due to the different amount of solvents associated with each GO sample. The observed significant weight loss at around 180 to 200 °C is attributed to the partial reduction of GO.

Insights into the Formation of LC GO. The self-assembly of amphiphiles in water is generally driven by hydrophobic interactions,[23−25] which is an important component of a larger solvophobic effect.[23,26−28] Studies into the thermodynamic driving force for the self-assembly of amphiphiles into LC phases have highlighted that the solvophobic force is almost always dominated by entropic contribution.[27,29] This behavior is very similar to hydrophobic forces in water where the nature of these interactions is entropic in origin as the enthalpy change is actually unfavorable in most cases.[30] Therefore, the process of self-assembly is an interplay of entropy and enthalpy terms in the free energy as given in eq 1.

$$\Delta G^{\circ}_{\text{self-assembly}} = \Delta H^{\circ}_{\text{self-assembly}} - T\Delta S^{\circ}_{\text{self-assembly}} \quad (1)$$

Other contributing factors are hydrogen bonding, van der Waals interactions, and electrostatic interactions.[30] Graphene oxide is typically considered as a negatively charged amphiphilic molecule, and as a result,[1,22,31,32] the $\Delta G^{\circ}_{\text{self-assembly}}$ in this case can be represented as the sum of the free energy change associated with hydrogen bonding, $\Delta G_{\text{hydrogen bond}}$, and electrostatic interactions, $\Delta G_{\text{electrostatic}}$ (see eq 2).

$$\Delta G^{\circ}_{\text{self-assembly}} = \Delta G_{\text{hydrogenbond}} + \Delta G_{\text{electrostatic}} \quad (2)$$

With water as the self-assembly medium, both factors contribute to the free energy change term. Only a few other solvents other than water are capable of supporting amphiphilc self-organization.[26,30,33,34] These solvents include a very limited range of multifunctional alcohols (such as ethylene glycol) and amides and a wide range of protic ionic liquids widely known as PILs.[26,30,33,34] With PILs, where the solvent itself is an ion, the surface charge screening results in negligible electrostatic contribution, which is in contrast with water or organic solvents where the electrostatic charges play an important role in the free energy associated with ordering.[30] In the case of LC GO, the solvent confined between the charged GO sheets adopts a more structural arrangement to balance the steric and repulsive forces. In this sense, GO can be considered as a self-assembling material due to the

fact that it involves supermolecular and supramolecular interactions such as electrostatic repulsion between the adjacent sheets and hydrogen bonding with the confined solvent molecules, which compensate for the loss of rotational entropy during the self-assembly process. Therefore, in the case of organic solvents, it is the interplay between the ability to form multiple hydrogen bonds and electrostatic charges, manifested through the Gordon Parameter, that governs the process of self-assembly.

The mechanism for the self-assembly process in organic solvents is considered to involve the solvophobic effect, which is linked to the solvent cohesiveness.[26] The Gordon parameter ($G = \gamma/V_{\text{m}}^{1/3}$) is a direct measure of the solvent cohesiveness where γ is the surface tension and V_{m} is the molar volume.[35] A high Gordon parameter represents first a higher chance to achieve self-assembled liquid crystalline phases and second a higher thermal stability.[36] However, the ultralarge size of GO sheets used in this study may push the boundaries toward organic solvents with Gordon parameters which are normally considered to be too low to be able to support solvophobic self-assembly. So far, the lowest reported Gordon parameter that supports amphiphilic self-assembly has been $G = 0.576$ J m^{-3} for a protic ionic liquid (EAB),[34] which is far beyond the limit predicted by Evans ($G \geq 1{-}1.2$ J m^{-3}).[37] However, as the Gordon parameter is directly dominated by surface tension and surface tension is a direct result of electrostatic charges and hydrogen bonding, in the case of PILs, the use of Gordon parameter might be irrelevant as the only dominating force is the ability of the liquid to form an extensive hydrogen bonding network. Recently, Drummond et al. also discovered that some low molecular weight amides can be utilized as self-assembly media with a Gordon value as low as 0.53 J m^{-3}, which is the direct result of the similarities between the chemical structure of PILs and the amides.[26] However, apart from these two groups of solvents, no other organic polar solvent with lower Gordon parameter less than 1.3 J m^{-3} is yet found to act as an amphiphilic self-assembly medium. However, employing ultralarge GO sheets has enabled us to achieve LC GO dispersions in a wide range of organic solvents with Gordon values previously deemed too low to support self-assembly. The list of solvents we have shown to support LC GO, along with Hansen parameters and Gordon parameter, are given in Table 2.

Apart from water which has a Gordon parameter higher than 1.2 J m^{-3}, DMF (which is an amide) shares a degree of structural similarity with PILs and can form extensive hydrogen bonded networks similar to water.[34] Therefore, although the Gordon parameter is very low, DMF could afford formation of LC GO. For the case of other solvents, it is evident that the ability to support LC GO is largely governed by the capability of

TABLE 2. Hansen Parameters and Gordon Parameter for the Solvents Could Support LC GO

| solvent	LC formation concentration (mg mL^{-1})	Hansen parameter for solvents				surface tension (mN m^{-1})	Gordon parameter (J m^{-3})
		dispersive	polar	hydrogen	total		
water	0.25	15.5	16.0	42.3	47.8	72.8	2.77
ethylene glycol	0.25	17.0	11.0	26.0	33.0	47.7	1.25
N-methyl pyrrolidone	0.25	18.0	12.3	7.20	23.0	40.8	0.890
DMF	0.25	17.4	13.7	11.3	24.9	37.0	0.869
dimethyl acetamide	0.25	16.8	11.5	10.2	22.8	36.7	0.810
CHP	0.25	18.2	6.80	6.50	20.5	42.3	0.770
methanol	0.25	15.1	12.3	22.3	29.6	22.7	0.661
THF	0.50	16.8	5.70	8.00	19.5	26.4	0.610
acetone	0.50	15.5	10.4	7.00	19.9	25.2	0.601
ethanol	0.25	15.8	8.80	19.4	26.5	22.1	0.569
isopropyl alcohol	0.25	15.8	6.10	16.4	23.6	23.0	0.542

the solvents to form hydrogen bonds. As an example, although the Gordon value of isopropyl alcohol and ethanol is very low (G = 0.541 and 0.569 J m^{-3}, respectively), their ability to form multiple hydrogen bonds, which is even much higher than DMF, can overcome the low cohesive energy density of the solvent. On the other hand, the lower ability of acetone and THF to form hydrogen bonds resulted in an increased GO concentration required for LC formation (0.50 mg mL^{-1}) compared to ethanol (0.25 mg mL^{-1}), which has a slightly lower Gordon parameter but much higher hydrogen bonding ability. As a result, it is safe to assume that the ability to form an extensive hydrogen bonding network is the most important parameter governing the self-organization process in the case of LC GO. Consequently, the interplay between the hydrogen bonding and the Gordon parameter can effectively determine (i) whether an organic solvent can induce the self-assembly process, and (ii) the lowest possible concentration in which spontaneous self-organization can occur.

Exploitation of the Self-Assembly Nature of LC GO. The intrinsic self-assembly nature of LC materials can be used to exploit them as versatile templates for the synthesis and alignment of nanoparticles.[11,14] We utilized LC GO to induce liquid crystallinity to SWNT dispersions through the addition of LC GO to the SWNT dispersions. Here we have investigated the effect of introducing SWNTs to LC GO dispersions. POM micrographs of LC GO-SWNTs are presented in Figure 4a,b, which shows the nematic LC behavior of as-prepared mixtures in CHP and DMF, respectively. Although SWNTs and rod-shaped particles under some specific conditions can form LC phases, this requires modification of the SWNTs' surface by biopolymers,[38,39] functionalization (with a subsequent compromise in electronic properties),[40,41] or the use of superacids.[42,43] Here we have dispersed SWNTs in CHP at concentrations as high as surfactant-assisted dispersions (1 mg mL^{-1}).[20] Subsequent mixing of this SWNT
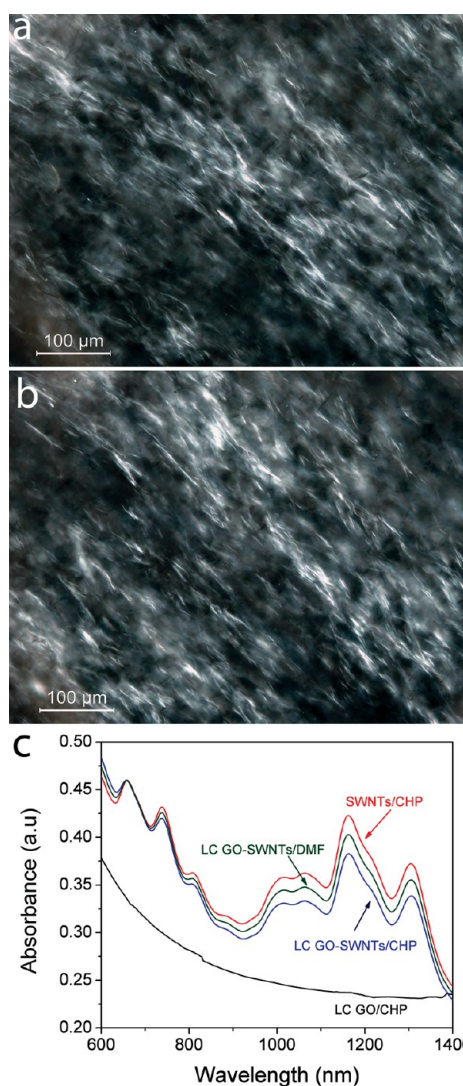
Figure 4. Representative POM micrographs of (a) LC GO-SWNTs/CHP (90:10 at ~1 mg mL^{-1}), (b) LC GO-SWNTs/DMF (90:10 at ~1 mg mL^{-1}). (c) UV/vis−near-IR spectra of SWNTs and LC GO dispersions before and after mixing together.

dispersion with CHP- or DMF-based lyotropic LC GO resulted in birefringence yet preserves the fundamental
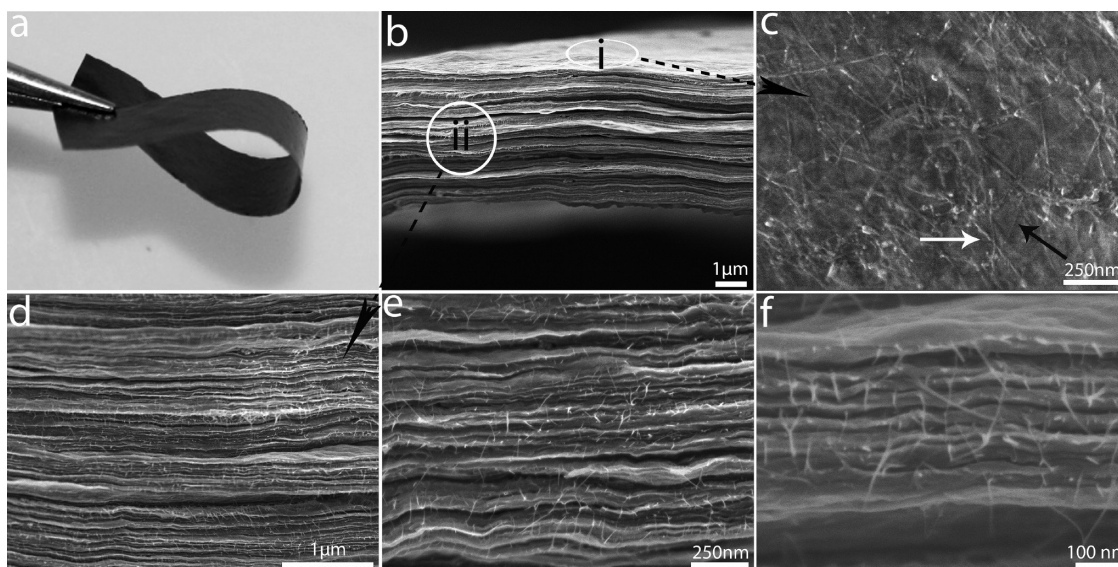
Figure 5. (a) Representative photograph of a flexible free-standing paper of LC GO-SWNT made by cast drying method. (b) SEM image of the cross section of as-cast dried LC GO-SWNT paper. (c) SEM image of the surface of the layer-by-layer composite, which is marked as region (i) in (b). Some of the SWNTs are laid on the surface of the paper (white arrow), while others are placed between layers of GO sheets (black arrow). Transparency of the monolayer/few layers of GO sheets allows observing tube sites in different layers. (d–f) Cross section of composite paper at different magnifications (marked as (ii) in (b)) confirmed the self-oriented nature of the composite as well as maintaining SWNTs debundled after the fabrication of composite.

properties of SWNTs (no dispersant was added). It has been shown that organic solvent-stabilized SWNT dispersions are sensitive to the presence of water whereby the addition of very small amounts of water will cause the dispersion to agglomerate and crash out of solution.[44] The water-free nature of our as-prepared LC GO in organic solvents is demonstrated by the fact that SWNTs do not agglomerate and crash out of the dispersion when they are added to the as-prepared LC GO in organic solvents. The quality of the dispersion even after addition of the GO is evidenced by the UV/vis–near-IR spectra (Figure 4c). The well-resolved interband transitions in the UV/vis–near-IR spectra of the SWNT dispersion before and after the addition of LC GO indicate that SWNT sizes are preserved in the composite formulation. According to Smalley and Hague,[45] UV/vis–near-IR spectroscopy is the most reliable method to determine SWNT size distribution based on Van Hove singularities. As is evident from UV/vis–near-IR spectra, the size of our nanotubes is predominantly in the range of 1 and 0.95 nm corresponding to the wavelength of ~1300 and ~1150 nm in the as-prepared SWNT dispersions, respectively. The quality of SWNT dispersions (bundle size) was also preserved during the combination with LC GO.

It is pertinent to mention that, although many particles can disturb the liquid crystal director field depending on the particle size, shape, and surface interaction with liquid crystal media,[46] GO in this regard enjoys a unique benefit. This unique benefit is due to minimizing the exert forces or torques in the direction perpendicular to the director to promote a configuration in which the distortion is minimal, leading to the in-plane alignment of anisotropic particles (the ordering of particles on GO planes) such as SWNTs, as evident from the strength of our as-prepared composite films (see next section). Prior to this work,[47−49] the only successful method of increasing the CNT concentration in lyotropic LCs has been through using extensive amounts of surfactants (which can adversely CNTs performance).[50] Only trace amounts of CNTs have been dispersed in thermotropic LCs in order to avoid CNT aggregation.[47,49] However, in our case, we have been able to disperse and organize substantial amounts of SWNTs (up to 10 wt %) in GO LC without losing birefringence properties and observing any aggregation. Therefore, this LC formulation was utilized for a facile fabrication of self-assembled layer-by-layer LC GO-SWNT 3D assemblies.

Self-Assembled Layer-by-Layer Multifunctional Composite. The LC properties of our as-prepared LC GO-SWNT dispersions in organic solvents induce a spontaneous self-assembly into engineered long-range-ordered layer-by-layer 3D structures upon simple casting and drying, as shown in Figure 5. The ease of synthesis, much shorter processing time, and high scalability of this route in contrast with other layer-by-layer production methods (such as Langmuir–Blodgett deposition) offer the opportunity for facile fabrication of 3D frameworks with exceptional properties. The excluded volume generated by large GO sheets for SWNTs results in an entropic rearrangement to form long-range ordering. Therefore, LC GO in CHP can be employed as a dispersing media to process SWNTs
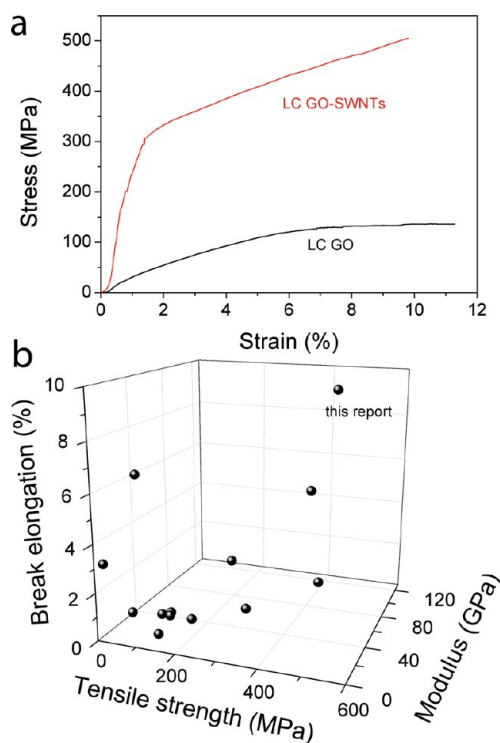
Figure 6. (a) Stress−strain curves of LC GO and LC GO-SWNT self-assembled composite. (b) Diagram of mechanical performance data for layer-by-layer nanocomposites and carbon-based neat papers and fibers in selected significant published reports and in this study (see also Table S1).

based on hydrophobic and $\pi-\pi$ interactions as well as a medium in which SWNTs can be self-assembled. This can consequently result in the fabrication of highly aligned and macroscopically periodic self-assembled structures of GO-SWNT hybrid material. The aggregate-free nature of our as-prepared LC GO-SWNTs enabled us to achieve an ultrastiff, ultrastrong layer-by-layer 3D architecture with high elongation-at-break which enjoys an average modulus of 51.3 GPa, tensile strength of 505 MPa, and elongation-at-break of 9.8% (Figure 6), which is much higher than the parent GO architecture.

The average strength, reported here, is much higher than those reported for bucky papers,[51] GO and rGO papers (prepared by either filtration or casting strategies) and fibers (either as-is or cross-linked),[17,52−55] paper-like materials based on vermiculite,[56] flexible graphite foil,[57,58] neat SWNT fibers,[42,43,55,59,60] and even layer-by-layer assembled polymer,[61] SWNTs,[62] or MWNT nanocomposites.[63] As proposed by Ruoff *et al.*, very high mechanical strength can be obtained if ordering and alignment of fibrils/macromolecules are achieved.[52] In comparison with irregularly laid-down individual fibrils obtained *via* filtration, the LC route provided us with a self-mediated platform to organize and order SWNTs resulting in an extraordinarily high mechanical strength. Our average modulus is also considerably higher than all those (Figure 6b and Table S1) and just inferior to either SWNT fiber composites with polymers or extensively processed SWNTs.[43,55,64]

The as-prepared composite paper exhibited an exceptional conductivity of 1500 S m^{-1}.

The ultralarge nature of our as-prepared GO sheets (with the average lateral size of 37 μm compared to typically a few hundred nanometers in the case of other reports) provides us with a highly wrinkled topography,[1,65] which can first contribute to an overall increase in strain and second maximize the fraction of the surface area available for mechanical reinforcement and toughening.[52,55] Therefore, in the case of ultralarge GO sheets, the initial straightening due to wrinkled topography plays a crucial role in the observed increase in elongation-at-break of our as-prepared GO compared to other reports. Furthermore, this enhanced wrinkled topography provides us with a unique platform to accommodate individual, separated SWNTs between the GO sheets, resulting in an overall enhancement in exploitation of the extraordinary mechanical properties of SWNTs. Also, the introduction of SWNTs can prevent the restacking of individual two-dimensional GO sheets, further enhancing the properties of the hybrid material. Furthermore, our GO-SWNT hybrid material exhibited a very high toughness on the order of 20 J g^{-1}, which is almost 2 orders of magnitude higher than GO paper,[52] 3 orders of magnitude higher than pristine bucky paper[51,66] and flexible graphite foils, and even 7 times higher than GO/rGO fibers.[17] The flat fracture surface of our ruptured paper is evidence of the good material homogeneity and layer-by-layer nature of both our as-prepared neat and hybrid papers. The strong interfacial bonding in the case of our hybrid paper is also evident from the straight fracture surface in contrast to the rupture of bucky paper (Figure 5). In regards to mechanical properties, SWNTs act as bridging components between individual GO sheets (see high-magnification SEM micrographs in Figure 5d−f). As the GO sheets are not strongly attached together, reinforcing them with SWNTs can result in an overall increase in mechanical properties. SWNTs can bridge individual GO sheets and therefore increase the shear force between GO sheets. Furthermore, the most important limitation of using SWNTs as reinforcing agents is the intertube and interfacial slippage within bundles. The poor load transfer within bundles results in interfacial slippage as the effective moduli and strength for bundles are far below those expected for individual SWNTs. The individual nature of SWNTs reported in our study, as evident in high-resolution SEM figures presented in Figure 5 and the well-resolved interband transitions in the UV/vis−near-IR spectra of the SWNT dispersion before and after the addition of LC GO presented in Figure 4, ensures that the shear slippage of nanotubes within the bundle does not occur and the mechanical properties of SWNTs used in this study are preserved, resulting in an overall enhancement of the final composite properties. The findings presented

here will pave the way to versatile and highly scalable routes for the fabrication of a wide range of large-scale 3D graphene-based architectures (including metallic or polymer-based composites) with extensive applications in multifunctional wearables, sensors, supercapacitor devices, and electronic gadgets.

CONCLUSION

In summary, our discovery of lyotropic LC GO dispersions in a range of organic solvents contributes to the fundamental understanding of the solvophobic effect and the parameters affecting the self-assembly process. The ability of the solvents to promote self-assembly in GO is governed by their polarity and is linked to the ability to form extensive hydrogen bonding. The steric hindrance between the highly charged GO sheets is the factor that overcomes the unfavorable loss of rotational entropy associated with ordering. The expansion of the list of known solvents that can promote the self-assembly process and lyotropic liquid crystallinity has enabled us to tailor-make processable self-assembled, self-oriented SWNTs/GO hybrid composites with superior mechanical performances (Table S1). This discovery could provide practical solutions to the processability of a wide range of materials that require organic solvents because of solubility issues and/or water sensitivity (*i.e.*, metal oxides, polymers, and nanomaterials).

METHODS

LC GO Synthesis. In order to obtain fully oxidized graphite and preserve the high initial lateral sizes of graphite flakes, dry expandable graphite flakes (3772, Asbury Graphite Mills USA) were first thermally treated at 1050 °C for 15 s. The resultant expanded graphite (EG) was used as the precursor for GO synthesis following previously described methods.[1,65,67] Briefly, 5 g of EG and 1 L of sulfuric acid were mixed and stirred in a flask for 24 h. Then 50 g of $KMnO_4$ was added to the mixture dropwise. The mixture was transferred into an ice bath, and 1 L of Milli-Q water and 250 mL of H_2O_2 were poured slowly into the mixture, realizing a color change of the suspension to light brown. Having been stirred for another 30 min, the GO particles were then washed and centrifuged with a HCl solution (9:1 water/HCl by volume), then centrifuged again and washed with Milli-Q water until the pH of the solution became about 5−6. The resultant ultralarge GO sheets were dispersed in deionized water by gentle shaking (*i.e.*, without the aid of sonication process).

N,*N*-Dimethylformamide (DMF), *N*-cyclohexyl-2-pyrrolidone (CHP), tetrahydrofuran (THF), acetone, ethylene glycol, *N*-methyl pyrrolidone (NMP), dimethyl acetamide (DMAc), methanol, isopropyl alcohol, and absolute ethanol, all from Sigma, have been chosen for investigation. LC GO dispersions in various organic solvents were prepared by extraction of water from the parent aqueous LC GO dispersion *via* repeated centrifugation−washing steps (6 times of 10−30 min at 11 000 rpm, ProSciTech TG16WS) using the selected solvent. Briefly, 15 mL of the parent aqueous LC GO (2.5 mg mL^{-1}) was poured into a 50 mL centrifuge tube (Nalgene centrifuge tube) to which 20 mL of the selected solvent was added and then mixed vigorously by vortex shaking. After centrifugation, 30 mL of the supernatant was extracted, replaced with 30 mL of the selected solvent, and then mixed vigorously by vortex shaking. This process was repeated 5 times to replace the water with the selected organic solvent.

Layer-by-Layer Self-Assembly of the LC GO-SWNT Composite. SWNT dispersion was prepared by adding 15 mg of HiPCO-SWNTs to 15 mL of CHP. This dispersion was subjected to a 3 h of high-power tip sonication (SONICS Vibra Cell 500 W, 30% amplitude) followed by a 1 day low-power bath sonication (Branson B5500R-DTH). The SWNTs/CHP (1 mg mL^{-1}) dispersion was then mixed with LC GO in DMF or in CHP (2.5 mg mL^{-1}) at the weight ratio of (10:90) followed by 10 min of vortex mixing. A self-assembled layer-by-layer composite was fabricated by casting 2 mL of the composite formulation into a Teflon mold (2 cm × 2 cm) and then oven-dried at 110 °C for 2 days. The resultant oven-dried GO-SWNT paper was washed several times by DMF and acetone and dried in air to remove the remaining solvent. GO paper, as the control, was made using GO in DMF; however, the SWNT in CHP did not form free-standing paper using simple casting.

Characterizations. AFM analysis was carried out by first depositing GO sheets from their dispersions on a precleaned and silanized silicon wafer (300 nm SiO_2 layer). Silane solution was prepared by mixing 3-aminopropyltriethoxysilane (Sigma) with water (1:9 vol) and one drop of hydrochloric acid (Sigma). Precut silicon substrates were silanized by immersing them in aqueous silane solution for 30 min and then washed thoroughly with Millipore water. LC GO in each solvent was first diluted to ∼50 μg mL^{-1}, then GO sheets were deposited onto silanized silicon substrates by immersing a silicon substrate into the GO dispersion for 5 s, then immersed in the solvent bath (the same solvent used to form the LC GO) for 30 s and then dried under nitrogen flow at room temperature. The CHP-based sample was then heated to 70 °C to be dried due to its higher boiling point compared to the other solvents. Prior to AFM analysis, GO sheets were observed under an optical microscope to ensure that uniform GO sheet deposition was achieved. Atomic force microscopy (MFP-3D AFM Asylum Research, CA) was carried out in tapping mode under ambient conditions. X-ray diffraction (XRD) studies were performed using a powder XRD system (Philips1825) with Cu Kα radiation ($\lambda = 0.154$ nm) operating at 40 keV and with a cathode current of 20 mA. Thermal gravimetric analyses (TGA) were carried out in nitrogen atmosphere from room temperature to 250 °C at a temperature ramp rate of 1 °C min^{-1}. The birefringence of LC GO dispersions was examined by polarized optical microscopy (POM, Leica CTR 6000) operated in transmission mode by looking at a drop of LC GO on a glass slide. UV/vis−near-IR spectra were recorded using a Shimadzu UV-3600 spectrometer from 600 to 1400 nm. The conductivity of LC GO-SWNT paper was measured using a JANDEL four-point probe resistivity system (model RM2) with a linear four-point probe head. The mechanical properties of the composite paper were measured using a Shimadzu tensile tester (EZ-S) at a strain rate of 0.5% min^{-1} parallel to the GO plane in the paper. Youngs modulus (Y), tensile strength (σ), breaking strain (ε), and breaking energy (toughness) were calculated, and the average was reported for 10 samples. The thickness of the composite papers was ∼10 μm, and the papers were cut 20 mm by 5 mm. The obtained strips were mounted on aperture cards with commercial superglue and allowed to air-dry. Note, only 10 mm of each sample was exposed to the applied strain as 5 mm from each side is used for gluing to the aperture card.

Supporting Information Available: Calculation of the theoretical concentration for LC formation. Figures S1–S6, representative polarized optical micrographs of LC GO dispersions in different solvents at various GO concentrations. Figure S7, XRD pattern of LC GO/SWNTs composite. Table S1, comparison of LC GO/SWNT mechanical performance data with layer-by-layer nanocomposites and carbon-based neat papers and fibers in selected significant previous reports and in this study. This material is available free of charge *via* the Internet at http://pubs.acs.org.

REFERENCES AND NOTES

1. Aboutalebi, S. H.; Gudarzi, M. M.; Zheng, Q. B.; Kim, J.-K. Spontaneous Formation of Liquid Crystals in Ultralarge Graphene Oxide Dispersions. *Adv. Funct. Mater.* **2011**, *21*, 2978–2988.

2. Dan, B.; Behabtu, N.; Martinez, A.; Evans, J. S.; Kosynkin, D. V.; Tour, J. M.; Pasquali, M.; Smalyukh, I. I. Liquid Crystals of Aqueous, Giant Graphene Oxide Flakes. *Soft Matter* **2011**, *7*, 11154–11159.

3. Guo, F.; Kim, F.; Han, T. H.; Shenoy, V. B.; Huang, J.; Hurt, R. H. Hydration-Responsive Folding and Unfolding in Graphene Oxide Liquid Crystal Phases. *ACS Nano* **2011**, *5*, 8019–8025.

4. Kim, J. E.; Han, T. H.; Lee, S. H.; Kim, J. Y.; Ahn, C. W.; Yun, J. M.; Kim, S. O. Graphene Oxide Liquid Crystals. *Angew. Chem., Int. Ed.* **2011**, *50*, 3043–3047.

5. Eda, G.; Chhowalla, M. Graphene Patchwork. *ACS Nano* **2011**, *5*, 4265–4268.

6. Xu, Z.; Gao, C. Aqueous Liquid Crystals of Graphene Oxide. *ACS Nano* **2011**, *5*, 2908–2915.

7. Behabtu, N.; Lomeda, J. R.; Green, M. J.; Higginbotham, A. L.; Sinitskii, A.; Kosynkin, D. V.; Tsentalovich, D.; Parra-Vasquez, A. N. G.; Schmidt, J.; Kesselman, E.; *et al.* Spontaneous High-Concentration Dispersions and Liquid Crystals of Graphene. *Nat. Nanotechnol.* **2010**, *5*, 406–411.

8. Hu, X.; Xu, Z.; Gao, C. Multifunctional, Supramolecular, Continuous Artificial Nacre Fibres. *Sci. Rep.* **2012**, *2*, 767.

9. Zamora-Ledezma, C.; Puech, N.; Zakri, C.; Grelet, E.; Moulton, S. E.; Wallace, G. G.; Gambhir, S.; Blanc, C.; Anglaret, E.; Poulin, P. Liquid Crystallinity and Dimensions of Surfactant-Stabilized Sheets of Reduced Graphene Oxide. *J. Phys. Chem. Lett.* **2012**, *3*, 2425–2430.

10. Fong, C.; Le, T.; Drummond, C. J. Lyotropic Liquid Crystal Engineering-Ordered Nanostructured Small Molecule Amphiphile Self-Assembly Materials by Design. *Chem. Soc. Rev.* **2012**, *41*, 1297–1322.

11. Bisoyi, H. K.; Kumar, S. Liquid-Crystal Nanoscience: An Emerging Avenue of Soft Self-Assembly. *Chem. Soc. Rev.* **2011**, *40*, 306–319.

12. Hamley, I. W. Nanotechnology with Soft Materials. *Angew. Chem., Int. Ed.* **2003**, *42*, 1692–1712.

13. Lagerwall, J. P. F.; Scalia, G.; New, A. Era for Liquid Crystal Research: Applications of Liquid Crystals in Soft Matter Nano-, Bio- and Microtechnology. *Curr. Appl. Phys.* **2012**, *12*, 1387–1412.

14. Dellinger, T. M.; Braun, P. V. Lyotropic Liquid Crystals as Nanoreactors for Nanoparticle Synthesis. *Chem. Mater.* **2004**, *16*, 2201–2207.

15. Kijima, T.; Yoshimura, T.; Uota, M.; Ikeda, T.; Fujikawa, D.; Mouri, S.; Uoyama, S. Noble-Metal Nanotubes (Pt, Pd, Ag) from Lyotropic Mixed-Surfactant Liquid-Crystal Templates. *Angew. Chem., Int. Ed.* **2004**, *43*, 228–232.

16. Hulvat, J. F.; Stupp, S. I. Anisotropic Properties of Conducting Polymers Prepared by Liquid Crystal Templating. *Adv. Mater.* **2004**, *16*, 589–592.

17. Xu, Z.; Gao, C. Graphene Chiral Liquid Crystals and Macroscopic Assembled Fibres. *Nat. Commun.* **2011**, *2*, 571.

18. Yousefi, N.; Gudarzi, M. M.; Zheng, Q.; Aboutalebi, S. H.; Sharif, F.; Kim, J.-K. Self-Alignment and High Electrical Conductivity of Ultralarge Graphene Oxide-Polyurethane Nanocomposites. *J. Mater. Chem.* **2012**, *22*, 12709–12717.

19. Krishnan, D.; Kim, F.; Luo, J.; Cruz-Silva, R.; Cote, L. J.; Jang, H. D.; Huang, J. Energetic Graphene Oxide: Challenges and Opportunities. *Nano Today* **2012**, *7*, 137–152.

20. Bergin, S. D.; Sun, Z.; Streich, P.; Hamilton, J.; Coleman, J. N. New Solvents for Nanotubes: Approaching the Dispersibility of Surfactants. *J. Phys. Chem. C* **2009**, *114*, 231–237.

21. Dimiev, A. M.; Alemany, L. B.; Tour, J. M. Graphene Oxide. Origin of Acidity, Its Instability in Water, and a New Dynamic Structural Model. *ACS Nano* **2013**, *7*, 576–588.

22. Medhekar, N. V.; Ramasubramaniam, A.; Ruoff, R. S.; Shenoy, V. B. Hydrogen Bond Networks in Graphene Oxide Composite Paper: Structure and Mechanical Properties. *ACS Nano* **2010**, *4*, 2300–2306.

23. Southall, N. T.; Dill, K. A.; Haymet, A. D. J. A View of the Hydrophobic Effect. *J. Phys. Chem. B* **2001**, *106*, 521–533.

24. Chandler, D. Interfaces and the Driving Force of Hydrophobic Assembly. *Nature* **2005**, *437*, 640–647.

25. Meyer, E.; Rosenberg, K. J.; Israelachvili, J. Recent Progress in Understanding Hydrophobic Interactions. *Proc. Natl. Acad. Sci. U.S.A.* **2006**, *103*, 8.

26. Greaves, T. L.; Weerawardena, A.; Drummond, C. J. Nanostructure and Amphiphile Self-Assembly in Polar Molecular Solvents: Amides and the "Solvophobic Effect". *Phys. Chem. Chem. Phys.* **2011**, *13*, 9180–9186.

27. Ray, A. Solvophobic Interactions and Micelle Formation in Structure Forming Nonaqueous Solvents. *Nature* **1971**, *231*, 313–315.

28. Akhter, M. S. Studies on Solvophobic Interactions and Micelle Formation in Non Aqueous Solvents. *Colloids Surf., A* **1999**, *150*, 25–30.

29. Evans, D. F.; Yamauchi, A.; Roman, R.; Casassa, E. Z. Micelle Formation in Ethylammonium Nitrate, a Low-Melting Fused Salt. *J. Colloid Interface Sci.* **1982**, *88*, 89–96.

30. Greaves, T. L.; Drummond, C. J. Ionic Liquids as Amphiphile Self-Assembly Media. *Chem. Soc. Rev.* **2008**, *37*, 1709–1726.

31. Withers, N. Graphene Oxide: Surfactant Sheets. *Nat. Chem.* **2010**, 10.1038/nchem.741.

32. Kim, J.; Cote, L. J.; Kim, F.; Yuan, W.; Shull, K. R.; Huang, J. Graphene Oxide Sheets at Interfaces. *J. Am. Chem. Soc.* **2010**, *132*, 8180–8186.

33. Ray, A. Micelle Formation in Pure Ethylene Glycol. *J. Am. Chem. Soc.* **1969**, *91*, 6511–6512.

34. Greaves, T. L.; Weerawardena, A.; Fong, C.; Drummond, C. J. Many Protic Ionic Liquids Mediate Hydrocarbon-Solvent Interactions and Promote Amphiphile Self-Assembly. *Langmuir* **2006**, *23*, 402–404.

35. Evans, D. F. Self-Organization of Amphiphiles. *Langmuir* **1988**, *4*, 3–12.

36. Lee, W. B.; Mezzenga, R.; Fredrickson, G. H. Anomalous Phase Sequences in Lyotropic Liquid Crystals. *Phys. Rev. Lett.* **2007**, *99*, 187801.

37. del Mar Graciani, M.; Muñoz, M.; Rodríguez, A.; Moyá, M. L. Water–*N,N*-Dimethylformamide Alkyltrimethylammonium Bromide Micellar Solutions: Thermodynamic, Structural, and Kinetic Studies. *Langmuir* **2005**, *21*, 3303–3310.

38. Moulton, S. E.; Maugey, M.; Poulin, P.; Wallace, G. G. Liquid Crystal Behavior of Single-Walled Carbon Nanotubes Dispersed in Biological Hyaluronic Acid Solutions. *J. Am. Chem. Soc.* **2007**, *129*, 9452–9457.

39. Badaire, S.; Zakri, C.; Maugey, M.; Derré, A.; Barisci, J. N.; Wallace, G.; Poulin, P. Liquid Crystals of DNA-Stabilized Carbon Nanotubes. *Adv. Mater.* **2005**, *17*, 1673–1676.

40. Song, W.; Kinloch, I. A.; Windle, A. H. Nematic Liquid Crystallinity of Multiwall Carbon Nanotubes. *Science* **2003**, *302*, 1363.

41. Zhang, S.; Kinloch, I. A.; Windle, A. H. Mesogenicity Drives Fractionation in Lyotropic Aqueous Suspensions of Multiwall Carbon Nanotubes. *Nano Lett.* **2006**, *6*, 568–572.

42. Davis, V. A.; Parra-Vasquez, A. N. G.; Green, M. J.; Rai, P. K.; Behabtu, N.; Prieto, V.; Booker, R. D.; Schmidt, J.; Kesselman, E.; Zhou, W.; *et al.* True Solutions of Single-Walled Carbon Nanotubes for Assembly into Macroscopic Materials. *Nat. Nanotechnol.* **2009**, *4*, 830–834.

43. Ericson, L. M.; Fan, H.; Peng, H.; Davis, V. A.; Zhou, W.; Sulpizio, J.; Wang, Y.; Booker, R.; Vavro, J.; Guthy, C.; *et al.* Macroscopic, Neat, Single-Walled Carbon Nanotube Fibers. *Science* **2004**, *305*, 1447–1450.

44. Sun, Z.; O'Connor, I.; Bergin, S. D.; Coleman, J. N. Effects of Ambient Conditions on Solvent−Nanotube Dispersions: Exposure to Water and Temperature Variation. *J. Phys. Chem. C* **2009**, *113*, 1260–1266.

45. Chiang, I. W.; Brinson, B. E.; Smalley, R. E.; Margrave, J. L.; Hauge, R. H. Purification and Characterization of Single-Wall Carbon Nanotubes. *J. Phys. Chem. B* **2001**, *105*, 1157–1161.

46. Hegmann, T.; Qi, H.; Marx, V. Nanoparticles in Liquid Crystals: Synthesis, Self-Assembly, Defect Formation and Potential Applications. *J. Inorg. Organomet. Polym. Mater.* **2007**, *17*, 483–508.

47. Lagerwall, J.; Scalia, G.; Haluska, M.; Dettlaff-Weglikowska, U.; Roth, S.; Giesselmann, F. Nanotube Alignment Using Lyotropic Liquid Crystals. *Adv. Mater.* **2007**, *19*, 359–364.

48. Lagerwall, J. P. F.; Scalia, G. Carbon Nanotubes in Liquid Crystals. *J. Mater. Chem.* **2008**, *18*, 2890–2898.

49. Lynch, M. D.; Patrick, D. L. Organizing Carbon Nanotubes with Liquid Crystals. *Nano Lett.* **2002**, *2*, 1197–1201.

50. Zeng, Q.; Cheng, J.; Tang, L.; Liu, X.; Liu, Y.; Li, J.; Jiang, J. Self-Assembled Graphene−Enzyme Hierarchical Nanostructures for Electrochemical Biosensing. *Adv. Funct. Mater.* **2010**, *20*, 3366–3372.

51. Sweetman, L. J.; Nghiem, L.; Chironi, I.; Triani, G.; in het Panhuis, M.; Ralph, S. F. Synthesis, Properties and Water Permeability of SWNT Buckypapers. *J. Mater. Chem.* **2012**, *22*, 13800–13810.

52. Dikin, D. A.; Stankovich, S.; Zimney, E. J.; Piner, R. D.; Dommett, G. H. B.; Evmenenko, G.; Nguyen, S. T.; Ruoff, R. S. Preparation and Characterization of Graphene Oxide Paper. *Nature* **2007**, *448*, 457–460.

53. Park, S.; Dikin, D. A.; Nguyen, S. T.; Ruoff, R. S. Graphene Oxide Sheets Chemically Cross-Linked by Polyallylamine. *J. Phys. Chem. C* **2009**, *113*, 15801–15804.

54. Chen, H.; Müller, M. B.; Gilmore, K. J.; Wallace, G. G.; Li, D. Mechanically Strong, Electrically Conductive, and Biocompatible Graphene Paper. *Adv. Mater.* **2008**, *20*, 3557–3561.

55. Shin, M. K.; Lee, B.; Kim, S. H.; Lee, J. A.; Spinks, G. M.; Gambhir, S.; Wallace, G. G.; Kozlov, M. E.; Baughman, R. H.; Kim, S. J. Synergistic Toughening of Composite Fibres by Self-Alignment of Reduced Graphene Oxide and Carbon Nanotubes. *Nat. Commun.* **2012**, *3*, 650.

56. Ballard, D. G. H.; Rideal, G. R. Flexible Inorganic Films and Coatings. *J. Mater. Sci.* **1983**, *18*, 545–561.

57. Reynolds Iii, R. A.; Greinke, R. A. Influence of Expansion Volume of Intercalated Graphite on Tensile Properties of Flexible Graphite. *Carbon* **2001**, *39*, 479–481.

58. Leng, Y.; Gu, J.; Cao, W.; Zhang, T.-Y. Influences of Density and Flake Size on the Mechanical Properties of Flexible Graphite. *Carbon* **1998**, *36*, 875–881.

59. Kozlov, M. E.; Capps, R. C.; Sampson, W. M.; Ebron, V. H.; Ferraris, J. P.; Baughman, R. H. Spinning Solid and Hollow Polymer-Free Carbon Nanotube Fibers. *Adv. Mater.* **2005**, *17*, 614–617.

60. Steinmetz, J.; Glerup, M.; Paillet, M.; Bernier, P.; Holzinger, M. Production of Pure Nanotube Fibers Using a Modified Wet-Spinning Method. *Carbon* **2005**, *43*, 2397–2400.

61. Podsiadlo, P.; Kaushik, A. K.; Arruda, E. M.; Waas, A. M.; Shim, B. S.; Xu, J.; Nandivada, H.; Pumplin, B. G.; Lahann, J.; Ramamoorthy, A.; *et al.* Ultrastrong and Stiff Layered Polymer Nanocomposites. *Science* **2007**, *318*, 80–83.

62. Shim, B. S.; Zhu, J.; Jan, E.; Critchley, K.; Kotov, N. A. Transparent Conductors from Layer-by-Layer Assembled Swnt Films: Importance of Mechanical Properties and a New Figure of Merit. *ACS Nano* **2010**, *4*, 3725–3734.

63. Olek, M.; Ostrander, J.; Jurga, S.; Möhwald, H.; Kotov, N.; Kempa, K.; Giersig, M. Layer-by-Layer Assembled Composites from Multiwall Carbon Nanotubes with Different Morphologies. *Nano Lett.* **2004**, *4*, 1889–1895.

64. Dalton, A. B.; Collins, S.; Munoz, E.; Razal, J. M.; Ebron, V. H.; Ferraris, J. P.; Coleman, J. N.; Kim, B. G.; Baughman, R. H. Super-Tough Carbon-Nanotube Fibres. *Nature* **2003**, *423*, 703–703.

65. Aboutalebi, S. H.; Aminorroaya-Yamini, S.; Nevirkovets, I.; Konstantinov, K.; Liu, H. K. Enhanced Hydrogen Storage in Graphene Oxide-Mwcnts Composite at Room Temperature. *Adv. Energy Mater.* **2012**, *2*, 1439–1446.

66. Titelman, G. I.; Gelman, V.; Bron, S.; Khalfin, R. L.; Cohen, Y.; Bianco-Peled, H. Characteristics and Microstructure of Aqueous Colloidal Dispersions of Graphite Oxide. *Carbon* **2005**, *43*, 641–649.

67. Aboutalebi, S. H.; Chidembo, A. T.; Salari, M.; Konstantinov, K.; Wexler, D.; Liu, H. K.; Dou, S. X. Comparison of GO, GO/MWCNTs Composite and MWCNTs as Potential Electrode Materials for Supercapacitors. *Energy Environ. Sci.* **2011**, *4*, 1855–1865.